Microwave-Based Sensor for the Noninvasive and Real-Time Analysis of 3-D Biological Microtissues: Microfluidic Improvement and Sensitivity Study

Olivia Peytral-Rieu, David Dubuc, Katia Grenier

Microwave-Based Sensor for the Non-Invasive and Real Time Analysis of 3D Biological Microtissues: Microfluidic Improvement and Sensitivity Study

Olivia Peytral-Rieu, *Student Member, IEEE,* David Dubuc, *Member, IEEE* and Katia Grenier, *Member, IEEE*

***Abstract*—Microwave dielectric spectroscopy of biological materials is gaining of interest as it presents attractive features such as being non-invasive, rapid, label-free and suitable for intracellular investigations, notably for biological and medical researches. Specific microwave biosensors have consequently been developed to investigate biomolecules, cells in suspension and also tissues. A type of biosensor is however missing for the analysis of 3D aggregates of cells, also called microtissues or spheroids, which constitute an intermediate biological model between 2D cell cultures and tissues or organs. Therefore, we present a microwave-based microsensor suitable for the study of such 3D biological models. It is composed of a coplanar waveguide (CPW) with a central capacitive gap, which allows to measure the capacitive and conductive contrasts between the studied bio-object and a reference liquid, typically the cell culture medium, in the frequency range from 500 MHz to 20 GHz. This sensor also integrates a microfluidic channel to maintain the microtissues in liquid. Two fluidic configurations are investigated, one open and one closed, the latter including a mechanical trap. The advantages of the closed configuration are then highlighted experimentally, enabling accurate and real-time microwave measurements of microtissues maintained in their culture medium and in the vicinity of the sensing area for sensitivity enhancement. In addition, an analytical study on the capacitive gap size performed with both simulations and experiments leads to an optimal gap size for sensitivity improvement. This new sensor consequently offers new non-invasive, non-destructive and dielectric sensing possibilities for biomedical investigations such as drug screening, personalized medicine and also fundamental research.**

***Index Terms*—Biology, coplanar waveguide, dielectric spectroscopy, microwave biosensor microtechnology, microtissues, spheroids.**

I. Introduction

ELECTRICAL approaches, especially dielectric spectroscopy techniques, which exploit the interaction between electromagnetic fields and materials, present attractive interests for a broad range of researches including biological ones [1]–[3]. RadioFrequency (RF) impedancemetry and microwave dielectric spectroscopy are gaining increasing attention for noninvasive, nondestructive biological investigations, while being label-free and cost-effective [4]–[7]. Electromagnetic waves in the microwave frequency range gather in particular significant interests for biological detection investigations. First, the wavelengths are larger or similar to the dimensions of the living and biological materials under test, resulting in a large variety of possible biological materials to study [8], ranging from nanoscale elements to tissues and body investigations. Appropriate electromagnetic instrumentations are therefore available to analyze biological phenomena according to the dielectric properties of the matter. In addition, water, which is the largest constituent of any biological materials or living cells [9], presents its dielectric relaxation in the microwave frequency range (around 20 GHz at ambient temperature), due to its molecular reorientation dynamic. Water molecules are then used as a natural marker of living organisms with microwave dielectric spectroscopy. Finally, this frequency range allows electromagnetic waves to bypass the bilipid cell membrane, giving access to intracellular investigations.

Microwave dielectric spectroscopy has therefore been demonstrated for detecting amino acids, carbohydrates, proteins, and nucleic acids in aqueous solutions, as well as cell suspensions without any requirement of pretreatment, labeling, fixation and/or permeabilization [10]–[18]. Moreover, it may also detect differences between treated and untreated cells (and yeasts) [19], [20], making it a promising method for testing drug effects. Drug screening in oncology is particularly important to identify potential molecules, that could effectively eliminate tumors. These tumors also constitute specific three-dimensional (3D) biological objects with their own defense bio-

Manuscript received XXX XX, 2023; revised XXX X, 2023; accepted XXX X, XXXX. This work was supported in part by LAAS-CNRS micro and nanotechnologies platform member of the French RENATECH network.
(Corresponding author: Olivia Peytral-Rieu)
O. Peytral-Rieu, D. Dubuc are with the LAAS-CNRS, Université de Toulouse, CNRS, Université Paul Sabatier, Toulouse, France (e-mails : opeytral@laas.fr, dubuc@laas.fr).
K. Grenier is with the LAAS-CNRS, Université de Toulouse, CNRS, Toulouse, France (e-mail: grenier@laas.fr).

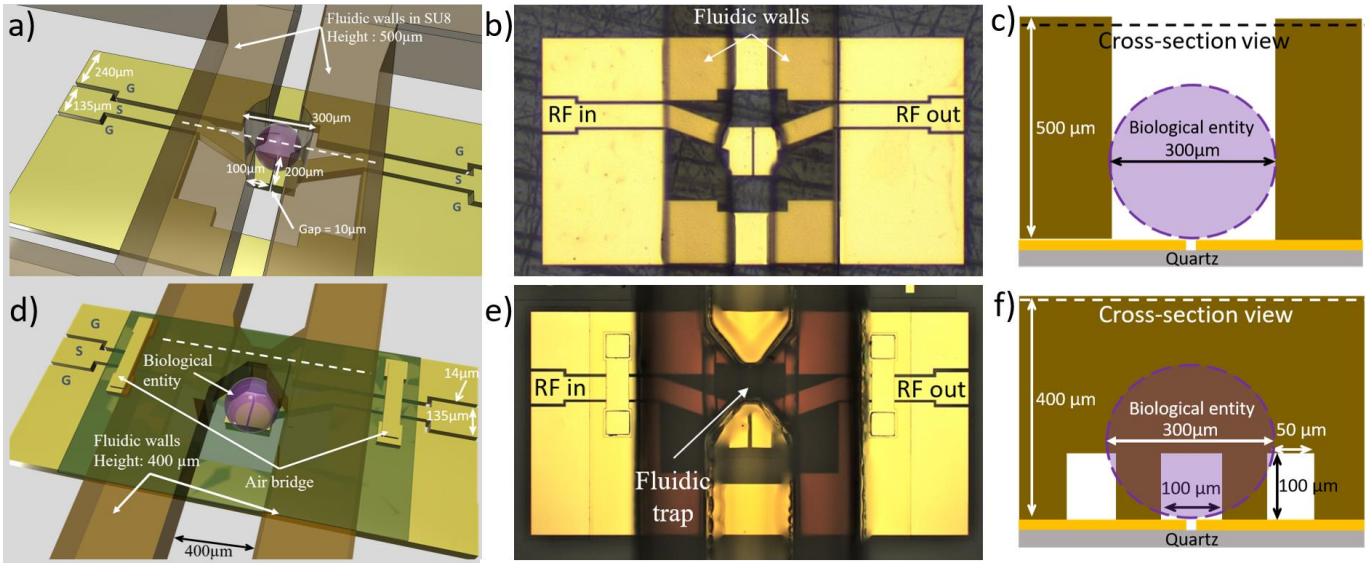

Fig. 1. Presentation of the two versions of the microwave sensor. Schematics of the CPW structures with a) an open fluidic configuration and d) a closed fluidic one, with the gold layer in yellow, the SU8 passivation in green, the fluidic system in brown. Photographs of b) the open fluidic and e) the closed fluidic structures. c) and f) Cross sections of c) the open fluidic and f) the closed fluidic structures, at the location marked by the dotted line in a) and d). The purple sphere or circle represent a 300 µm diameter 3D biological entity. The grey color corresponds to the wafer substrate, while the yellow layer to gold electrodes.

mechanisms.

When a molecule is tested in drug screening, the results must be as accurate as possible, while using biological models as close as possible to the real conditions and environment. Traditionally, 2D cultured cells are used for such experiments, due to their ease of preparation and affordability, although such models are now considered to be quite far from the heterogeneity and the complexity of the *in vivo* configuration. Mastered 3D cell aggregates, also called spheroids or microtissues, have consequently been introduced, constituting a new intermediate biological model between 2D cultured cells and *in vivo* investigations [21]. They present both the advantages of 2D cell cultures, i.e a rapid and affordable growth, and those of an *in vivo* configuration, with its specific complexity of environment and structure. Moreover, the size of the microtissues gives access to different models of tumor. Indeed, when the microtissues are larger than 200 µm in diameter, a hypoxic core (dead cells) is formed, inducing the formation of different layers in the spheroid, a necrotic one in the center, while external and living cells may spread [21]–[23].

From the study of individual cells to that of organs, including cells in suspension, numerous microwave based-devices exist both in fluidic or other configurations [24]–[29]. However, for the intermediate size of microtissues, none have been introduced at this particular frequency range. Only a first version of a microwave-based sensor dedicated to the determination of the dielectric properties of spheroids of 300 µm in diameter in the frequency range from 500 MHz to 20 GHz was introduced in [30]. This structure exhibits an open fluidic configuration, which leads to significant measurement dispersions due on the one hand to a lack of precision in the position of the microtissue within the sensor and on the other hand to intrinsic evaporation. To overcome these drawbacks, a complete revised version of the sensor is proposed and quantitatively evaluated in this article. It now integrates a hydrodynamic trapping solution to precisely locate the spheroid under test in the close vicinity of the microwave sensing zone and a close microfluidic channel with inlet and outlet, enabling a continuous liquid flow and avoiding any possible evaporation phenomenon. To better highlight the improvements provided by this entirely revised sensor configuration, the first sensor is briefly reminded to understand the disadvantages that motivated the development of the new sensor integrating a fluidic advanced structure. A comparison study is then carried out using both sensor configurations loaded with a liquid medium and with polystyrene beads. To do so, the electrical modeling employed to extract the capacitive and conductive contrasts of the microwave measurements is previously given. Finally, an analytical study of the capacitive gap used to sense the biological element is provided to define the best dimensions of the device to maximize sensitivity.

II. Microwave Sensor Description and Fluidic Optimization

A. Description of the Microwave Sensor and Test Setup

Fig. 1(a) to (c) and Fig. 1(d) to (f) present the schematics and the photographs of the RF biosensors with open and closed fluidic configurations respectively. They are based on a coplanar waveguide with a capacitive gap of 10-µm width located in the center of the structure. The positioning of the coplanar probes is achieved with 50 Ohm accesses, which present a central conductor of 135 µm wide and slots of 14 µm large. As far as the closed fluidic configuration is concerned, the grounds are also balanced with air bridges. For both structures, the sensing gap is placed just below the object under test in the middle of the coplanar line. While considering the fluidic configurations, the open structure presented in Fig. 1(b) and c) implies to maintain the object under test with the circular shape of the open fluidic wall only, as shown in the cross section of Fig. 1(c). Two reservoirs are placed on each side of

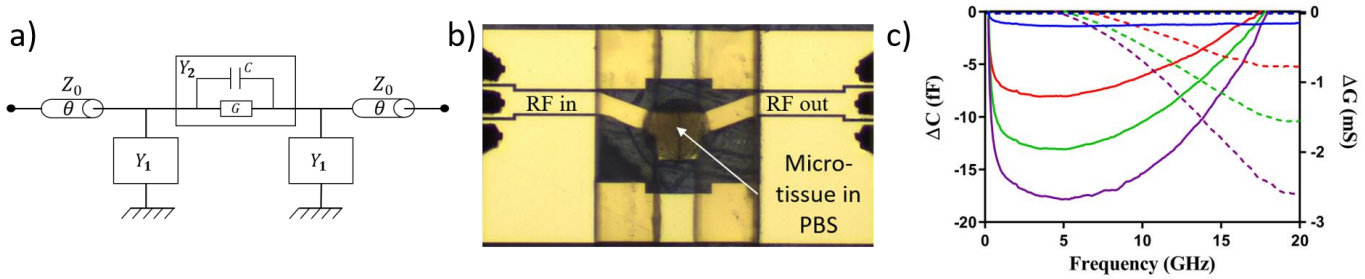

Fig. 2. a) Equivalent electrical circuit used for data analysis. b) Photograph of the open-fluidic structure loaded with a microtissue. c) Extracted mean value of the capacitive and conductive contrasts obtained for three different spheroids and the PBS reference fluid. Spheroids 1, 2 and 3 are indicated by the red, green and purple curves and present a diameter of 262 µm, 266 µm and 364 µm respectively. The solid lines correspond to the capacitive contrasts ΔC, while the dotted lines are for the conductive contrasts ΔG.

the bio-element location through two narrowed fluidic channels in order to maintain the spheroid in liquid during experiments. As for the fluidic advanced structure, the view of Fig 1(e) shows how the biological object is blocked by a funnel shape in the fluidic channel, allowing its precise placement by continuous fluidic flow in the mechanical trap.

To characterize the fabricated microdevice, this latter is connected to a Vector Network Analyzer using two coplanar probes and two coaxial cables, using a preliminary SOLT calibration step. Measurements are performed from 500 MHz to 20 GHz.

B. *Fluidic Configuration of the Sensor*

In order to maintain the spheroid under test in its culture medium during the experiments, the first microwave device presented in [30] has an open channel with two reservoirs on each side. The spheroid placement has to be manual in this configuration and the medium can evaporate. Consequently, dispersions of the dielectric measurements exist. To overcome these two issues, a closed fluidic system is fabricated with the object blocked by a permanent flow and a mechanical trap placed just above the sensing gap. This trap includes three openings. The central one is larger than the two others placed on each side and serves as a guide to the object to be analyzed. The side openings allow the fluid to flow while the central one is closed by the object under test, as indicated by the cross-section of the structure in Fig. 1(f).

For experiments, the fluid channel is loaded with a Phosphate Buffered Saline (PBS) solution at a flow rate of 5 µL/min.

C. *Microfabrication of the Device*

The fabrication of the microwave biosensor involves standard microtechnology processes. First, the sensor is made on a quartz substrate, which is previously cleaned with a piranha process and an oxygen plasma treatment. The metallization used to define the microwave coplanar waveguide is then performed with a lift-off technique. The obtained waveguide is composed of a titanium flash to enable the metal adhesion to the substrate, followed by an evaporated gold layer of 0.3 µm thick.

A patterning of a photosensitive SU-8 polymer layer is then carried out to obtain a passivation on the device, except at the location of the coplanar accesses and of the sensing gap. A second metallization is also done to create air bridges with the same process as that described for the coplanar waveguide.

The next step is dedicated to the elaboration of the fluidic part with the creation of both the spheroid blocker and fluidic channel. These are realized with the superposition and patterning of several dry photoresist films. The total height of the fluidic walls corresponds to 400 µm thick and the top lid to 100 µm thick respectively.

D. *Electrical Modeling and Dielectric Contrasts Calculation*

As the microwave biosensor is a two-port system, an electrical model is defined, as indicated in Fig. 2(a). It includes (1) two-line sections with a characteristic impedance Z_0 associated with a phase θ, (2) two normalized admittances which correspond to the microfluidic channels y_1 (= Y_1Z_0), also considered to be symmetrical with respect to the sensing zone, and (3) y_2 (= Y_2Z_0), the normalized admittance of our object under test, also modeled by a capacitor, C, and a conductance, G, placed in a shunt configuration. S_{11} and S_{21} corresponds to the measured S parameters when the structure is loaded with a bio-entity, whereas $S_{11\text{empty}}$ and $S_{21\text{empty}}$ are the S parameters while the device is empty. As explained in [30] and considering $\theta = 0$, y_2 may be expressed as:

$$y_2 = \frac{1}{2}\left(\frac{1-\frac{S_{11}-S_{21}}{S_{11empty}}}{1+\frac{S_{11}-S_{21}}{S_{11empty}}} - y_1\right), \quad (1)$$

Where

$$y_1 = \frac{1-\frac{S_{11}+S_{21}}{S_{11empty}}}{1+\frac{S_{11}+S_{21}}{S_{11empty}}}. \quad (2)$$

Using the calculated y_1 and y_2, one may extract the C capacitor and the G conductance, which model the object under test with Eq. 3 and Eq. 4 respectively:

$$C = \frac{1}{2\pi f}\frac{Img(y_2)}{50}, \quad (3)$$

$$G = \frac{Re(y_2)}{50}, \quad (4)$$

where f is the frequency.

To better enhance electrical variations between the host medium and the entity under test, electrical contrasts are considered. Those capacitive and conductive contrasts are obtained using Eq. 5 and Eq. 6 respectively, where C_{DUT} and G_{DUT} are the capacitance and the conductance of the device under test when loaded by an object to be analyzed and C_{REF} and G_{REF} are the capacitance and the conductance obtained with a reference fluid in the sensor, respectively.

$$\Delta C = C_{DUT} - C_{REF} \quad (5)$$

$$\Delta G = G_{DUT} - G_{REF} \quad (6)$$

The measurements are consequently realized in two different steps, with first the measurement of the device with the reference fluid (here PBS) and then the measurement of the device with the biological object each minute during fifteen minutes.

This procedure is applied to both measured and simulated data. By way of example, Fig. 2(b) and (c) present the photograph of the open-fluidic structure loaded with a microtissue and the extracted mean values of the capacitive and conductive contrasts obtained for three different spheroids, respectively.

E. Experimental Evaluation of the Microfluidic Channel Modification

As explained in the section II.B, the initial microwave sensor presented in [30] includes an open fluidic channel. This configuration leads to several drawbacks. Here is evaluated the improvement expected by a closed microfluidic configuration. As the major dispersions with the first sensor are detected with polystyrene beads due to their low weight, this model is also kept in this investigation to better highlight the improvement of the closed fluidic structure.

To perform this evaluation, two beads in PBS are measured in the two fluidic configurations. Due to the dispersions in the available polystyrene beads, these may present slightly different diameters. Microwave measurements are recorded every minute for at least 20 minutes.

A double-regime stabilization is observed on both types of devices, open and closed. The first regime is related to the fluidic stabilization inside the system and lasts approximately 5 min. This first period is not considered in the remainder of this article. The extracted data referring to 0 minute consequently start after this stabilization.

TABLE I
COMPARISON BETWEEN THE OPEN AND CLOSED CONFIGURATIONS

	ΔC at 5GHz (fF)		ΔG at 20GHz (mS)	
	Mean	Standard deviation	Mean	Standard deviation
PBS opened	-1.09	0.57	-0.02	0.06
206 µm opened	-65.81	1.60	-10.38	0.22
260 µm opened	-63.81	5.61	-10.01	0.78
PBS closed	-1.14	0.15	-0.04	0.01
292 µm closed	-60.46	0.13	-5.81	0.02
212 µm closed	-64.12	0.07	-6.95	0.01

Mean values are calculated by considering the entire eleven-minutes period of the different measurements.

Only in open fluidic configuration, a second period of measurements is linked to the fluctuations induced by the bead movements in the structure. Such variations are not observed in the closed structure. Therefore, to be able to compare the two fluidic configurations, this second period is divided in two stages (0-5 min and 7-11 min), in order to consider the time needed for the final placement of the beads in the open fluidic structure.

The mean values and the standard deviation of the dielectric contrasts are calculated for each half period. The trajectories between the two periods are given in Fig. 3(a), (b) and (c) for the open structure and Fig. 3(d), (e) and (f) for the closed structure respectively. As the graphs present the same scales, the size of the trajectory arrows provides a quantitative

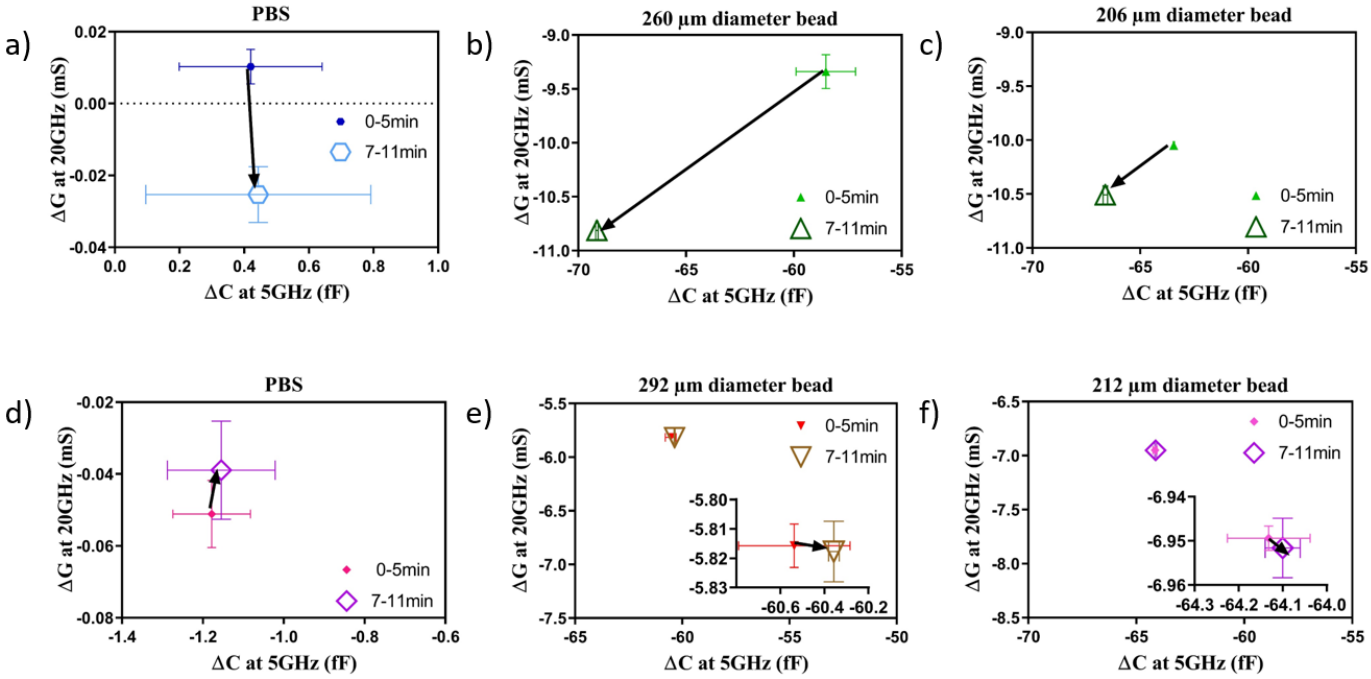

Fig. 3. Comparison of variations between dielectric contrasts with open (a, b, c) and closed (d, e, f) systems. a) and d) correspond to the measurements of PBS whereas b), c), e) and f) of polystyrene beads. The plain symbol corresponds to the data obtained during the 0-5 min period and the hollow one during the 7-11 min period. The arrows indicate the trajectories between the two time periods.

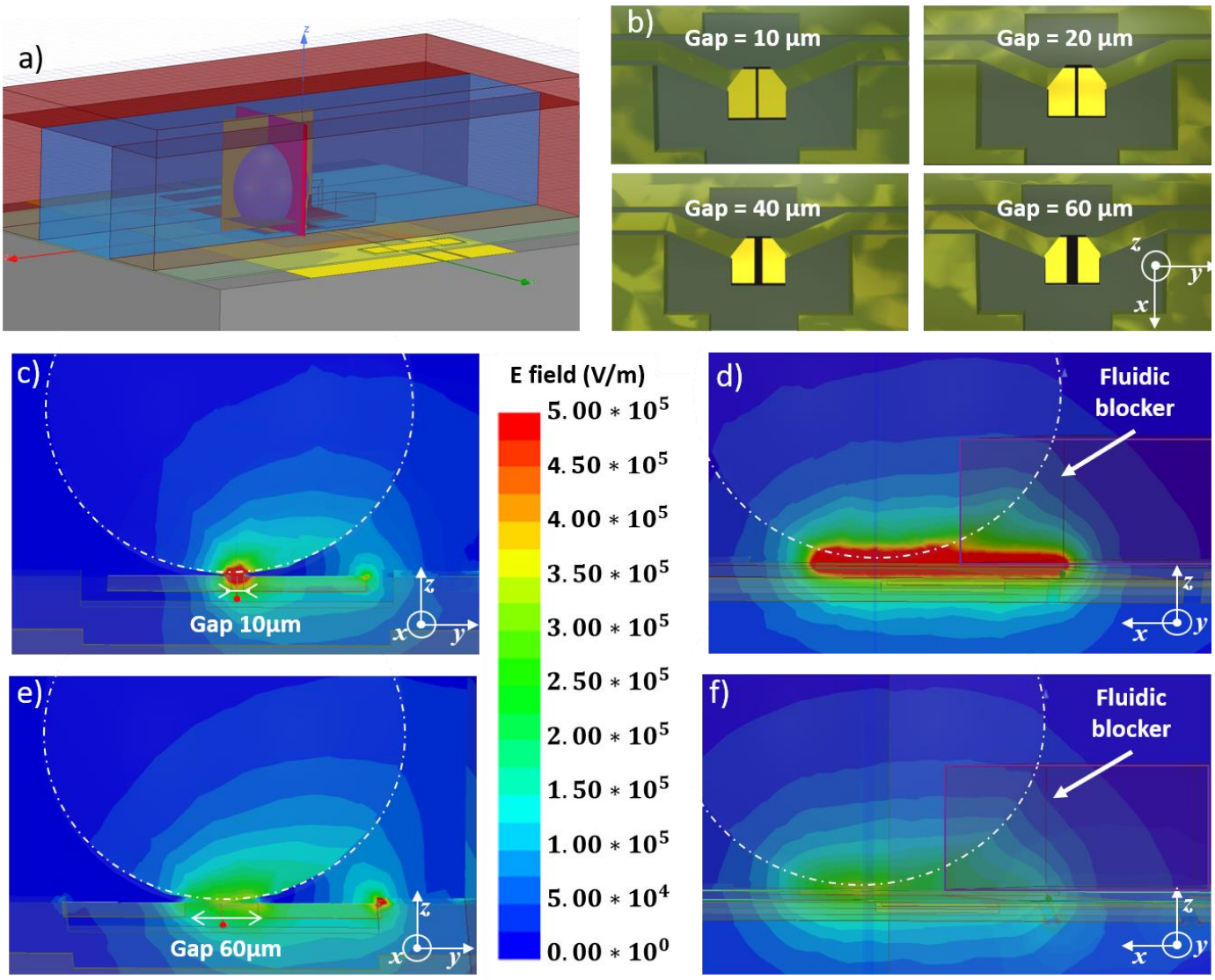

Fig.4. a) 3D view of the global system at scale with the electrodes in yellow on a quartz wafer in gray, the SU8 passivation in green, the fluidic system in red and the liquid medium in blue. A polystyrene bead placed in front of the fluidic blocker on the electrodes is symbolized in purple. The pink and brown planes crossing the spheroid represent the two sectional views of c), e) and d), f) respectively. b) Zoom on the sensing zone and the gap width *g* with the four different gaps tested. Representations of the electric field modulus for a gap width of 10 and 60 µm at 5 GHz obtained with HFSS along the (y,z) plane for c) and e) respectively, and along the (x,z) plane for d) and f). The white dotted line represents the border of the polystyrene bead.

information on the dispersions and the stability of the measurements. This figure clearly shows that the ΔC and ΔG variations of the open system are larger than those obtained with the closed system. The standard deviation of ΔG indeed presents a value ranging up of 0.78 mS with polystyrene beads in the open configuration, instead of 0.02 mS with the closed structure. Likewise, the standard deviation of ΔC is up to 5.61 fF and less than 0.21 fF for the respective settings. Moreover, the placement of the beads on the sensing gap is also faster and more efficient with the closed system.

A summary of these results is given in Table I with both mean values and standard deviations of ΔC and ΔG over an 11 minutes period. The low standard deviations in the case of the closed configuration confirms its superiority in term of stability of the microwave measurements in comparison with the open structure. The flow in the closed system indeed allows stable localization of the polystyrene bead at the bottom of the mechanical trap, in the close vicinity of the microwave electrodes. In addition, evaporation no longer has an influence. This new closed system is consequently more suitable for accurate measurements.

In addition to the fluidic improvement, an analytical study of the biosensor is performed to enhance its sensitivity.

III. Sensitivity Optimization of the Capacitive Sensing Gap

A previous study performed on a microwave biosensor dedicated to the analysis of individual cells [31] has already demonstrated the influence of the width of the capacitive gap on the sensitivity of the sensor. Therefore, to investigate a 10 µm-diameter cell, a structure with a 2 µm-width gap presents

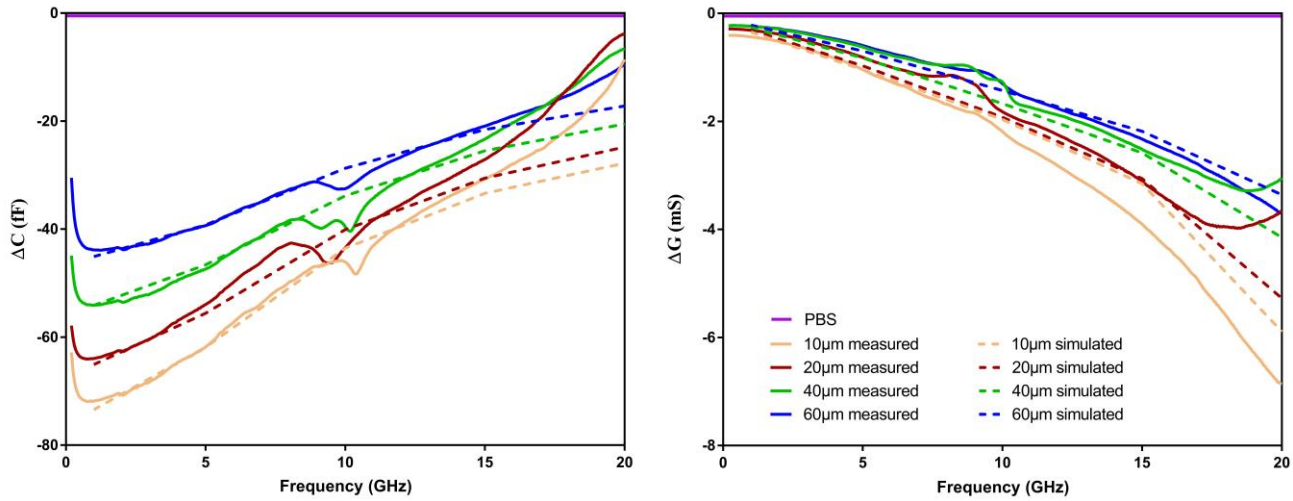

Fig. 5. Experimental mean values of the capacitive and conductive contrasts obtained for single polystyrene beads as a function of frequency for different gap widths (10, 20, 40 and 60 µm) for solid lines and simulation data in dotted line.

the highest sensitivity. However, the device presented in this paper aims at studying 3D biological object with a diameter close to 300 µm. An analytical study related to the impact on the sensitivity of the capacitive gap width is consequently conducted in order to determine the optimal value to achieve the maximum dielectric contrasts. A specific object model is initially defined.

A. Choice of the Object Model Under Study

The object, which is chosen to evaluate the influence of the gap on the sensitivity, corresponds to polystyrene beads with a diameter close to 300 µm. They are indeed easier to manipulate than microtissues during the microwave measurements performed to validate the analytic study. They present a round 3D shape, which is simple to implement in an electromagnetic software. Finally, due to the low permittivity of polystyrene compared to water-based biological entities, high dielectric contrasts are expected. The microtissues, which correspond to aggregates of cells and thus with constituents similar to those present in the host medium, indeed exhibit low dielectric contrasts compare to the reference fluid.

B. Simulations of the Microwave Sensor

To evaluate the influence of the gap width on the sensitivity of the device, 3D simulations using HFSS are performed at different frequencies (1 GHz, 5 GHz, 10 GHz, 15 GHz and 20 GHz). The schematic of the simulated structure is given in Fig. 4(a). Fig. 4(b) shows the different gaps tested. The permittivities of the different elements used for the simulations comes from [32]–[35]. Initially, the HFSS simulations are carried out to get the theorical *S* parameters of the empty device (S_{empty}) and then of the device loaded by the reference fluid (S_{11} and S_{21}). This enables to obtain the capacitance and conductance of the reference fluid, C_{REF} and G_{REF}, with the same calculation as described in section II.D. In a second phase, the *S* parameters of the device loaded with a polystyrene bead placed in the reference fluid are simulated to obtain the capacitance and the conductance of the device under test, i.e. C_{DUT} and G_{DUT} respectively, for the different gaps and frequencies of interest. Finally, the extracted capacitances and conductances are used to calculate the two capacitive and conductive contrasts, ΔC and ΔG, according to the gap sizes and frequencies.

The results of the simulations are presented in dotted lines in Fig. 5 and Fig. 6 for a 300 µm diameter bead. Fig. 5 presents the capacitive and conductive contrasts versus frequency, while Fig. 6 provides the capacitive and conductive contrasts versus the gap width at 5 GHz and 15 GHz respectively. Maximum contrasts in absolute value are observed for a width of 10 µm.

To confirm these results, experiments are conducted and described in the next section.

C. Experimental Results

The influence of the capacitive gap on the sensitivity of the device is tested with the closed fluidic configuration.

Due to microfabrication constraints, structures with a capacitive gap width equal to or greater than 10 µm are fabricated and tested, ranging from 10 to 60 µm. All devices are microfabricated on the same quartz wafer to limit microfabrication variations from batch to batch.

Three different beads are measured for each size of the capacitive gap. Each measurement is taken every minute for 15 min. As previously mentioned in section II.E, the first four minutes are not considered to allow the stabilization of the microwave measurements. The mean value and standard deviation for each gap width are then extracted based on the 10 minutes long measurements. These results are all gathered in Fig. 5 and Fig. 6 in solid lines.

Fig. 5 presents the mean value of the capacitive and conductive contrasts, ΔC and ΔG respectively, as a function of frequency. Each color corresponds to a gap width. The PBS measurement is used as the reference for the two contrasts. Similar to simulation results, the magnitudes of the dielectric contrasts decrease as the gap width rises, except for ΔG above 18 GHz. This result is confirmed by the curves indicated in Fig. 6, which presents the capacitive and conductive contrasts as a

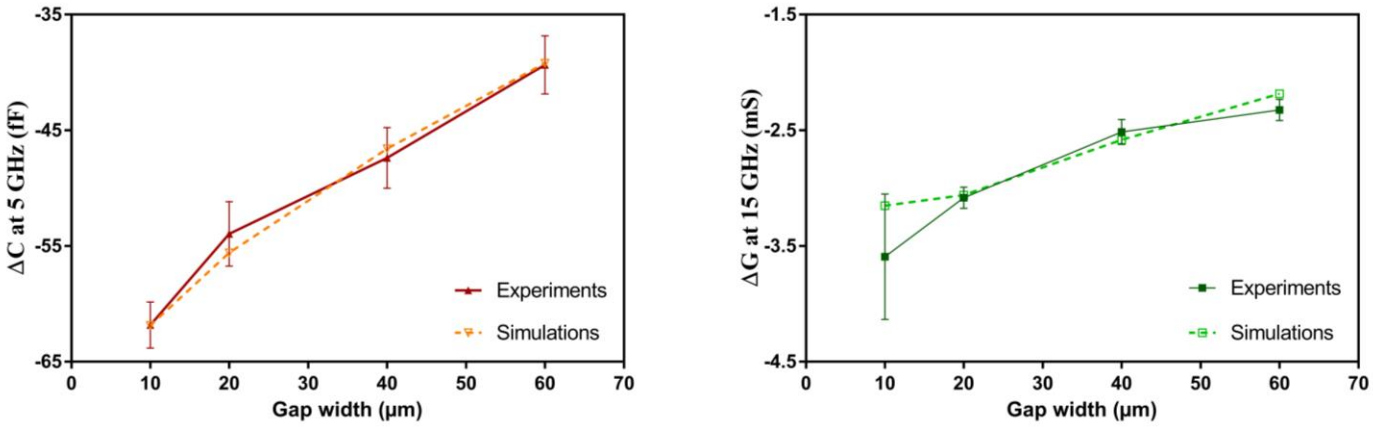

Fig. 6. Measured ΔC and ΔG in function of the gap width, at 5 GHz and 15 GHz respectively, associated with the simulated results. The standard deviation is calculated based on the measurement of three different polystyrene beads for each gap tested.

function of the gap width at 5 GHz and 15 GHz respectively. The greatest magnitude contrasts are obtained for a gap width of 10 µm. As visible with the 3D views of the electromagnetic simulations of Fig. 4, the electric field is more intense in the 10 µm wide gap and its vicinity in comparison to that of 60 µm (cf. Fig. 4(c) compare to Fig. 4(e). Even if the first temptation would have been to choose large capacitive gaps to better cope with samples size, smaller gaps should however be preferred to maximize the strength of the electromagnetic field, leading to better sensitivity of the elements under test.

IV. Conclusion

In this article, an optimized microwave sensor dedicated to the analysis of 3D biological models is described. Due to its closed fluidic configuration with an integrated mechanical trap to block microtissues in the immediate vicinity of the sensing area, the sensor operates both in flow and in real time. A comparison of this structure with the one having an open fluidic configuration clearly highlights the benefits of the new fluidic channel and micro-tissue trapping. A better stability of the microwave measurements is achieved as well as an improved reliability. Moreover, the placement of the microtissue to be tested is obtained more quickly and more efficiently with the closed fluidic system compare to the open one.

In addition, an analytical study of the capacitive sensing area is performed to define the best sensor dimension adapted to improve its sensitivity. Both simulations and experimental results carried out with polystyrene beads lead to the selection of a capacitive gap of 10 µm wide to reach the highest dielectric contrasts in amplitude.

Such a microwave sensor enables real time analysis of microtissues exhibiting a size close to 300 µm in diameter. Due to the configuration of the mechanical trap, the host medium of the spheroid may be modified during the microwave experiments. This capability is particularly interesting for drug screening investigations and opens up new perspectives in biology and medicine with the non-invasive and dielectric analysis of 3D biological models.

References

[1] R. D. Stoy, K. R. Foster, and H. P. Schwan, ‘Dielectric properties of mammalian tissues from 0.1 to 100 MHz; a summary of recent data’, *Phys. Med. Biol.*, vol. 27, no. 4, pp. 501–513, Apr. 1982, doi: 10.1088/0031-9155/27/4/002.

[2] E. C. Gregg and K. D. Steidley, ‘Electrical Counting and Sizing of Mammalian Cells in Suspension’, *Biophys. J.*, vol. 5, no. 4, pp. 393–405, Jul. 1965, doi: 10.1016/S0006-3495(65)86724-8.

[3] P. Mehrotra, B. Chatterjee, and S. Sen, ‘EM-Wave Biosensors: A Review of RF, Microwave, mm-Wave and Optical Sensing’, *Sensors*, vol. 19, no. 5, p. 1013, Feb. 2019, doi: 10.3390/s19051013.

[4] H. Thielecke, J. Fleckenstein, P. Bartholoma, and C. Rube, ‘Evaluation of impedance spectroscopy for the characterization of small biological samples in tissue-based test systems’, in *The 26th Annu. Int. Conf. of the IEEE Engineering in Medicine and Biology Society*, San Francisco, CA, USA: IEEE, 2004, pp. 2070–2073. doi: 10.1109/IEMBS.2004.1403608.

[5] T. Gerasimenko *et al.*, ‘Impedance Spectroscopy as a Tool for Monitoring Performance in 3D Models of Epithelial Tissues’, *Front. Bioeng. Biotechnol.*, vol. 7, p. 474, Jan. 2020, doi: 10.3389/fbioe.2019.00474.

[6] R. Pethig and D. B. Kell, ‘The passive electrical properties of biological systems: their significance in physiology, biophysics and biotechnology’, p. 38.

[7] F. Groeber *et al.*, ‘Impedance Spectroscopy for the Non-Destructive Evaluation of In Vitro Epidermal Models’, *Pharm. Res.*, vol. 32, no. 5, pp. 1845–1854, May 2015, doi: 10.1007/s11095-014-1580-3.

[8] H. P. Schwan, ‘Electrical properties of blood and its constitutents: Alternating current spectroscopy’, *Blut*, vol. 46, no. 4, pp. 185–197, Apr. 1983, doi: 10.1007/BF00320638.

[9] K. Grenier *et al.*, ‘Recent Advances in Microwave-Based Dielectric Spectroscopy at the Cellular Level for Cancer Investigations’, *IEEE Trans. Microw. Theory Tech.*, vol. 61, no. 5, pp. 2023–2030, May 2013, doi: 10.1109/TMTT.2013.2255885.

[10] K. Grenier, D. Dubuc, T. Chen, F. Artis, M. Poupot, and J.-J. Fournie, ‘Microwave dielectric spectroscopy: An emerging analyzing technique for biological investigations at the cellular level’, in *2013 IEEE Topical Conf. on Biomedical Wireless Technologies,*

Networks, and Sensing Systems, Austin, TX, USA: IEEE, Jan. 2013, pp. 40–42. doi: 10.1109/BioWireleSS.2013.6613668.

[11] D. Dubuc *et al.*, 'Microwave-based biosensor for on-chip biological cell analysis', *Analog Integr. Circuits Signal Process.*, vol. 77, no. 2, pp. 135–142, Nov. 2013, doi: 10.1007/s10470-013-0111-1.

[12] D. Faizullin, N. Zakharchenko, Y. Zuev, A. Puzenko, E. Levy, and Y. Feldman, 'Hydration of AMP and ATP Molecules in Aqueous Solution and Solid Films', *Int. J. Mol. Sci.*, vol. 14, no. 11, pp. 22876–22890, Nov. 2013, doi: 10.3390/ijms141122876.

[13] F. Artis, D. Dubuc, J.-J. Fournie, M. Poupot, and K. Grenier, 'Sub-microliter microwave dielectric spectroscopy for identification and quantification of carbohydrates in aqueous solution', in *2015 IEEE Topical Conf. on Biomedical Wireless Technologies, Networks, and Sensing Systems (BioWireleSS)*, San Diego, CA, USA: IEEE, Jan. 2015, pp. 1–3. doi: 10.1109/BIOWIRELESS.2015.7152125.

[14] E. Levy, G. Barshtein, L. Livshits, P. B. Ishai, and Y. Feldman, 'Dielectric Response of Cytoplasmic Water and Its Connection to the Vitality of Human Red Blood Cells: I. Glucose Concentration Influence', *J. Phys. Chem. B*, vol. 120, no. 39, pp. 10214–10220, Oct. 2016, doi: 10.1021/acs.jpcb.6b06996.

[15] X. Ma, X. Du, H. Li, X. Cheng, and J. C. M. Hwang, 'Ultra-Wideband Impedance Spectroscopy of a Live Biological Cell', *IEEE Trans. Microw. Theory Tech.*, vol. 66, no. 8, pp. 3690–3696, Aug. 2018, doi: 10.1109/TMTT.2018.2851251.

[16] A. C. Stelson *et al.*, 'Label-free detection of conformational changes in switchable DNA nanostructures with microwave microfluidics', *Nat. Commun.*, vol. 10, no. 1, p. 1174, Dec. 2019, doi: 10.1038/s41467-019-09017-z.

[17] G. Poiroux *et al.*, 'Label-free detection of mitochondrial activity with microwave dielectric spectroscopy', *Int. J. Biotechnol. Bioeng.*, 2020.

[18] S. Mohammadi, A. V. Nadaraja, K. Luckasavitch, M. C. Jain, D. J. Roberts, and M. H. Zarifi, 'A Label-Free, Non-Intrusive, and Rapid Monitoring of Bacterial Growth on Solid Medium Using Microwave Biosensor', *IEEE Trans. Biomed. Circuits Syst.*, vol. 14, no. 1, pp. 2–11, Feb. 2020, doi: 10.1109/TBCAS.2019.2952841.

[19] J. A. Osterberg *et al.*, 'Microwave Sensing of Yeast Cell Species and Viability', *IEEE Trans. Microw. Theory Tech.*, vol. 69, no. 3, pp. 1875–1886, Mar. 2021, doi: 10.1109/TMTT.2020.3048176.

[20] F. Artis *et al.*, 'Microwaving Biological Cells: Intracellular Analysis with Microwave Dielectric Spectroscopy', *IEEE Microw. Mag.*, vol. 16, no. 4, pp. 87–96, May 2015, doi: 10.1109/MMM.2015.2393997.

[21] S. Nath and G. R. Devi, 'Three-dimensional culture systems in cancer research: Focus on tumor spheroid model', *Pharmacol. Ther.*, vol. 163, pp. 94–108, Jul. 2016, doi: 10.1016/j.pharmthera.2016.03.013.

[22] J. Laurent, C. Frongia, M. Cazales, O. Mondesert, B. Ducommun, and V. Lobjois, 'Multicellular tumor spheroid models to explore cell cycle checkpoints in 3D', *BMC Cancer*, vol. 13, no. 1, p. 73, Dec. 2013, doi: 10.1186/1471-2407-13-73.

[23] C. Veelken, G.-J. Bakker, D. Drell, and P. Friedl, 'Single cell-based automated quantification of therapy responses of invasive cancer spheroids in organotypic 3D culture', *Methods*, vol. 128, pp. 139–149, Sep. 2017, doi: 10.1016/j.ymeth.2017.07.015.

[24] M. Lazebnik *et al.*, 'A large-scale study of the ultrawideband microwave dielectric properties of normal, benign and malignant breast tissues obtained from cancer surgeries', *Phys. Med. Biol.*, vol. 52, no. 20, pp. 6093–6115, Oct. 2007, doi: 10.1088/0031-9155/52/20/002.

[25] H. Li *et al.*, 'Differentiation of live and heat-killed E. coli by microwave impedance spectroscopy', *Sens. Actuators B Chem.*, vol. 255, pp. 1614–1622, Feb. 2018, doi: 10.1016/j.snb.2017.08.179.

[26] A. Tamra, M.-P. Rols, D. Dubuc, and K. Grenier, 'Impact of a chemical stimulus on two different cell lines through microwave dielectric spectroscopy at the single cell level', in *2019 IEEE MTT-S Int. Microwave Biomedical Conf. (IMBioC)*, Nanjing, China: IEEE, May 2019, pp. 1–4. doi: 10.1109/IMBIOC.2019.8777745.

[27] A. Tamra, M. Deburghgraeve, D. Dubuc, M.-P. Rols, and K. Grenier, 'Microwave dielectric spectroscopy for single cell irreversible electroporation monitoring', in *2016 IEEE MTT-S Int. Microwave Symp. (IMS)*, San Francisco, CA: IEEE, May 2016, pp. 1–4. doi: 10.1109/MWSYM.2016.7540429.

[28] R. Narang *et al.*, 'Sensitive, Real-time and Non-Intrusive Detection of Concentration and Growth of Pathogenic Bacteria using Microfluidic-Microwave Ring Resonator Biosensor', *Sci. Rep.*, vol. 8, no. 1, p. 15807, Oct. 2018, doi: 10.1038/s41598-018-34001-w.

[29] M. H. Zarifi, H. Sadabadi, S. H. Hejazi, M. Daneshmand, and A. Sanati-Nezhad, 'Noncontact and Nonintrusive Microwave-Microfluidic Flow Sensor for Energy and Biomedical Engineering', *Sci. Rep.*, vol. 8, no. 1, p. 139, Jan. 2018, doi: 10.1038/s41598-017-18621-2.

[30] O. Peytral-Rieu, K. Grenier, and D. Dubuc, 'Microwave Sensor Dedicated to the Determination of the Dielectric Properties of 3D Biological Models from 500MHz to 20GHz', in *2021 IEEE MTT-S Int. Microwave Symp. (IMS)*, Atlanta, GA: IEEE, Jun. 2021, p. 4.

[31] W. Chen, D. Dubuc, and K. Grenier, 'Parametric study of a microwave sensor dedicated to the dielectric spectroscopy of single particles and biological cells', in *2015 European Microwave Conf. (EuMC)*, Paris, France: IEEE, Sep. 2015, pp. 829–832. doi: 10.1109/EuMC.2015.7345892.

[32] T. Chen, F. Artis, D. Dubuc, J.-J. Fournié, M. Poupot, and K. Grenier, 'Microwave biosensor dedicated to the dielectric spectroscopy of a single alive biological cell in its culture medium', pp. 1–4, 2013, doi: 10.1109/MWSYM.2013.6697740.

[33] A. Ebberg *et al.*, 'Thin Glass Characterization in the Radio Frequency Range', in *Ceramic Transactions Series*, J. Akedo, T.-Y. Tseng, X. M. Chen, and H.-T.

Lin, Eds., Hoboken, NJ, USA: John Wiley & Sons, Inc., 2014, pp. 35–50. doi: 10.1002/9781118771402.ch4.
[34] N. Ghalichechian, 'Permittivity and Loss Characterization of SU-8 Films for mmW and Terahertz Applications', *IEEE ANTENNAS Wirel. Propag. Lett.*, vol. 14, p. 4, 2015.
[35] K. Grenier *et al.*, 'Integrated Broadband Microwave and Microfluidic Sensor Dedicated to Bioengineering', *IEEE Trans. Microw. THEORY Tech.*, vol. 57, no. 12, p. 8, 2009.

O. Peytral-Rieu (S'20, M'23) received M.S. degree in translational medicinal chemistry from University of Montpellier, Montpellier, France, in 2019; Engineering Degree in chemistry, biology and health from the Engineering Chemistry School of Montpellier, Montpellier, France, in 2019. She received the Ph.D. degree in Electromagnetic, Hyper Frequency systems from the University of Toulouse, Toulouse, France, in 2022. She is currently a Doctoral Fellow with the Laboratory of Analysis and Architecture of System, National Scientific Research Center, Toulouse. Her current research interests include the use of microwave based dielectric spectroscopy for the study and the characterization of microtissues. Dr. Peytral-Rieu is a member of the IEEE Microwave Theory and Technology Society (IEEE MTT-S), and member of the European Microwave Association (EuMA)

K. Grenier (S'99, M'03) received her M.S. and Ph.D. degrees in electrical engineering from the University of Toulouse, Toulouse, France, in 1997 and 2000, respectively. She was engaged in microelectromechanical systems (MEMS) circuits on silicon. She was a Postdoctoral Fellow at Agere Systems (Bell Labs). In 2001, she joined the Laboratory of Analysis and Architecture of System of the National Scientific Research Center (LAAS-CNRS), Toulouse, France. From 2007 to 2009, she was with the Laboratory for Integrated Micromechatronic Systems CNRS (LIMMS-CNRS)/Institute of Industrial Science (IIS), University of Tokyo, Tokyo, Japan, where she was engaged in launching research activities on microwave-based biosensors. Her research interests in LAAS-CNRS are focused on the development of fluidic-based microsystems, notably for biological and medical applications at the cellular and molecular levels.

She is the head of the High Frequency and Fluidic Micro-nanosystems Group (MH2F Group) at LAAS-CNRS. She has participated or organized several international events, including the 2020 MTT-S International Microwave Biomedical Conference (IMBioC 2020), where she has acted as General Chair. Dr. Grenier is a member of the European Microwave Association (EuMA) and a member of the IEEE Microwave Theory and Technology Society (IEEE MTT-S), and notably the IEEE MTT-28 Technical Committee on Biological effect and medical applications of RF and microwave of the IEEE MTT-S.

D. Dubuc (S'99, M'03) received the Agregation degree from the Ecole Normale Supérieure de Cachan, Paris, France, in 1996, and the M.S. and Ph.D. degrees in electrical engineering from the University of Toulouse, Toulouse, France, in 1997 and 2001, respectively. From 2002 to 2013, he was an Associate Professor with the University of Toulouse, and a Researcher with the Laboratory of Analysis and Architecture of System part of National Scientific Research Center (LAAS-CNRS), Toulouse, France. From 2007 to 2009, he was a Visiting Senior Researcher with the Laboratory of Integrated Micromechatronic Systems (LIMMS-CNRS)/Institute of Industrial Science (IIS), University of Tokyo, Tokyo, Japan. Since 2013, he has been Professor at the University of Toulouse. His research interests include the development of microwave circuits integrated with microtechnologies and their application to wireless telecommunication and biology.

He has participated or organized several international events, including GAAS 2005 and the 2020 MTT-S International Microwave Biomedical Conference (IMBioC 2020), where he has acted as Topical Committee Chair.

Prof. Dubuc is a member of the IEEE Microwave Theory and Technology Society (IEEE MTT-S), and member of the European Microwave Association (EuMA).